Journal of Pathology
J Pathol November 2023; **261**: 256–268
Published online 11 August 2023 in Wiley Online Library
(wileyonlinelibrary.com) DOI: 10.1002/path.6172

ORIGINAL ARTICLE

Comprehensive molecular characterization of adenoid cystic carcinoma reveals tumor suppressors as novel drivers and prognostic biomarkers

Marta Persson[1†], Mattias K Andersson[1†], Per-Erik Sahlin[2], Yoshitsugu Mitani[3], Margaret S Brandwein-Weber[4], Henry F Frierson Jr[5], Christopher Moskaluk[5], Isabel Fonseca[6], Renata Ferrarotto[7], Werner Boecker[8,9], Thomas Loening[9], Adel K El-Naggar[3] and Göran Stenman[1*]

[1] *Sahlgrenska Center for Cancer Research, Department of Pathology, University of Gothenburg, Gothenburg, Sweden*
[2] *Department of Plastic Surgery, Sahlgrenska University Hospital, Gothenburg, Sweden*
[3] *Department of Pathology, The University of Texas MD Anderson Cancer Center, Houston, TX, USA*
[4] *Department of Pathology, Icahn School of Medicine at Mount Sinai, New York, NY, USA*
[5] *Department of Pathology, University of Virginia Health System, Charlottesville, VA, USA*
[6] *Serviço de Anatomia Patológica, Instituto Português de Oncologia de Francisco Gentil – Lisboa and Instituto de Anatomia Patológica, Faculdade de Medicina de Lisboa, Lisbon, Portugal*
[7] *Department of Thoracic Head and Neck Medical Oncology, The University of Texas MD Anderson Cancer Center, Houston, TX, USA*
[8] *Gerhard Domagk Institute of Pathology, University of Muenster, Muenster, Germany*
[9] *Gerhard-Seifert Reference Centre, Hamburg, Germany*

**Correspondence to: G Stenman, Sahlgrenska Center for Cancer Research, Department of Pathology, University of Gothenburg, Box 425, 405 30 Gothenburg, Sweden. E-mail: goran.stenman@gu.se*

[†]These authors contributed equally to this work.

Abstract

Adenoid cystic carcinoma (ACC) is a MYB-driven head and neck malignancy with high rates of local recurrence and distant metastasis and poor long-term survival. New effective targeted therapies and clinically useful biomarkers for patient stratification are needed to improve ACC patient survival. Here, we present an integrated copy number and transcriptomic analysis of ACC to identify novel driver genes and prognostic biomarkers. A total of 598 ACCs were studied. Clinical follow-up was available from 366 patients, the largest cohort analyzed to date. Copy number losses of 1p36 (70/492; 14%) and of the tumor suppressor gene *PARK2* (6q26) (85/343; 25%) were prognostic biomarkers; patients with concurrent losses ($n = 20$) had significantly shorter overall survival (OS) than those with one or no deletions ($p < 0.0001$). Deletion of 1p36 independently predicted short OS in multivariate analysis ($p = 0.02$). Two pro-apoptotic genes, *TP73* and *KIF1B*, were identified as putative 1p36 tumor suppressor genes whose reduced expression was associated with poor survival and increased resistance to apoptosis. *PARK2* expression was markedly reduced in tumors with 6q deletions, and *PARK2* knockdown increased spherogenesis and decreased apoptosis, indicating that *PARK2* is a tumor suppressor in ACC. Moreover, analysis of the global gene expression pattern in 30 ACCs revealed a transcriptomic signature associated with short OS, multiple copy number alterations including 1p36 deletions, and reduced expression of *TP73*. Taken together, the results indicate that *TP73* and *PARK2* are novel putative tumor suppressor genes and potential prognostic biomarkers in ACC. Our studies provide new important insights into the pathogenesis of ACC. The results have important implications for biomarker-driven stratification of patients in clinical trials.

Keywords: tumor suppressor gene; transcriptomic profiling; TP73; prognostic biomarker; PARK2; MYB; genomic profiling; adenoid cystic carcinoma; 6q26 deletion; 1p deletion

Received 15 December 2022; Revised 19 June 2023; Accepted 28 June 2023

No conflicts of interest were declared.

Introduction

Adenoid cystic carcinoma (ACC) is an aggressive cancer that predominantly affects the head and neck but also occurs in the breast, tracheobronchial tree, skin, prostate, and female genital tract [1,2]. ACC is generally resistant to therapy, and there are no systemic treatments available for inoperable recurrent or metastatic tumors [3,4]. The prognosis for head and neck ACC is poor, and most patients with recurrent/metastatic tumors will die from their disease [1,5,6].

The genomic hallmark of ACC is a translocation-generated oncogenic gene fusion encoding the N-terminal part of the transcription factor MYB linked to the C-terminal part of the transcription factor NFIB [7–9]. In a subset of ACCs, *MYB* is replaced by *MYBL1* linked to *NFIB* or other fusion partners [10–12]. The MYB::NFIB fusion drives proliferation of ACC cells and is crucial for ACC spherogenesis [13,14]. Notably, the fusion is regulated by IGF1R in an AKT-dependent manner [13,15].

In contrast to the near-universal *MYB/MYBL1* activation in ACC, the frequency of other mutations in individual genes is low [2,13,16–24]. Nonetheless, certain mutations seem to cluster in specific pathways such as NOTCH and IGF/FGF signaling as well as in genes involved in chromatin remodeling. Further progress in understanding the molecular pathogenesis and clinical significance of recurrent genomic alterations in this enigmatic and aggressive cancer will require studies of larger well-characterized patient cohorts with long-term follow-up. Here, we used an integrated approach to study the copy number and transcriptomic profiles of a large cohort of ACC. Clinical follow-up was available from 366 patients, the largest cohort analyzed to date. We identified novel oncogenic drivers, including the tumor suppressor gene *PARK2* and pro-apoptotic genes in 1p36 whose reduced expression are associated with aggressive behavior and poor survival in ACC.

Materials and methods

Tumor material and patient data

Fresh frozen and formalin-fixed paraffin embedded (FFPE) tumor tissues were available from surgical specimens of 100 head and neck ACCs (supplementary material, Table S1). The genomic profiles of 40 of these have been reported [25]. In addition to the 100 ACC specimens, we also analyzed tissue microarrays (TMAs) containing 498 cases, bringing the total number of analyzed ACCs to 598 (supplementary material, Figure S1).

In the TMAs, each tumor was represented by at least two core biopsies. FFPE tissue blocks and TMA sections were obtained from the Departments of Pathology at University Medical Center Hamburg-Eppendorf, University of Texas MD Anderson Cancer Center, University of Alabama at Birmingham, University of Virginia Health System/Charlottesville, Instituto Português de Oncologia Francisco Gentil, and Sahlgrenska University Hospital in Gothenburg, Sweden. Survival data were available for 366 cases. In addition, we had access to the following clinicopathological parameters: sex, age, localization, stage, metastasis, and tumor grade (supplementary material, Table S2). Tumors were graded as lesions with no solid component (grade 1), <30% solid component (grade 2), and ≥30% solid component (grade 3) [26]. Only specimens with >70% tumor cellularity were used for genomic profiling.

Ethical statement

The study was approved by the ethics committee of Instituto Português de Oncologia Francisco Gentil – Lisboa (UIC-1042), the MD Anderson Cancer Center Institutional Review Board (IRB), the University of Virginia IRB, the University of Alabama at Birmingham IRB, and the regional ethics committee in Gothenburg (D-No: 178-08). The use of archived diagnostic leftover tissues for manufacturing of TMAs (Institute for Pathology, University Medical Center Hamburg-Eppendorf, Germany) and their analysis for research purposes was approved by local laws (HmbKHG, §12.1) and by the local ethics committee (Ethics Commission Hamburg, WF-049/09). The work was done in compliance with the Declaration of Helsinki.

Copy number profiling

Genomic DNA was isolated from fresh frozen tumor tissue ($n = 58$) and FFPE tumor tissue ($n = 42$) as described [25]. High-resolution array comparative genomic hybridization (arrayCGH) was done with the SurePrint G3 Human CGH Microarray 4X180K/244K oligonucleotide arrays (Agilent Technologies, Santa Clara, CA, USA) as recommended by the manufacturer [27]. The data were analyzed with Nexus Copy Number software version 8.1 (BioDiscovery, El Segundo, CA, USA) using the FASST2 segmentation algorithm to define nonrandom regions of copy number alterations (CNAs) across the genome. The significance threshold for segmentation was $p = 1.0\text{E-}6$ for fresh frozen tumors and $p = 1.0\text{E-}8$ for FFPE tumors. Similarly, the log2 ratio thresholds for gains and losses were 0.25 and −0.2 for fresh frozen tumors and 0.3 and −0.3 for FFPE tumors, respectively. Each aberration was checked manually to confirm the accuracy of the call. Sex chromosomes and regions partially or completely covered by a copy number variation in the Database of Genomic Variants (http://dgvbeta.tcag.ca/dgv/app/news?ref=NCBI36/hg19) were not analyzed [28]. GISTIC2.0 was used to identify genomic regions significantly gained/amplified/deleted [29]. The Benjamini–Hochberg method was used to correct for false discovery rate (FDR), and regions with Q values <0.05 were considered significant. CNAs present in 10 or more cases (10%) were considered recurrent. The arrayCGH data are available for download from the Gene Expression Omnibus (GEO) database (https://ncbi.nlm.nih.gov/geo/, Accession No. GSE153228).

Fluorescence *in situ* hybridization (FISH)

FISH analysis of TMAs was done to study CNAs involving 1p36 represented by the marker genes *CHD5* (1p36.31; *CHD5*/1q44 subtelomeric deletion probe from Cytocell, Cambridge, UK), *KLHDC7A* (1p36.13; *KLHDC7A*/CEN1 probe from Abnova, Taipei, Taiwan),

and *PARK2* (6q26) (PARK2 FISH probe from Empire Genomics (Buffalo, NY, USA) and a subtelomeric 6qter probe from Leica Biosystems, Nussloch, Germany), as previously described [24,27]. The protocols for pretreatment, hybridization, and posthybridization washes were as recommended by the manufacturers. Cell nuclei were stained with DAPI. Fluorescence signals were digitized, processed, and analyzed with the CytoVision image-analysis system (Applied Imaging, San Jose, CA, USA) and Isis FISH imaging system version 5.5 (MetaSystems, Altlussheim, Germany). At least 20 nuclei were scored from each core biopsy.

Global gene expression and RT-qPCR analyses

RNA was extracted from fresh frozen ACCs ($n = 30$; these cases were also analyzed by arrayCGH; see supplementary material, Table S1) and normal salivary glands (NSGs) ($n = 7$) and analyzed using Human Gene 1.0 ST gene chips (Affymetrix, Santa Clara, CA, USA), as previously described [13]. Differential global gene expression, hierarchical clustering, and principal component analyses were done with Nexus Expression 3.0 (BioDiscovery) and RStudio 1.1.463 with the limma package [30] and 'hclust' and 'prcomp' functions. FDR-corrected Q values <0.05 (Benjamini–Hochberg) were considered significant. Gene ontologies were analyzed with Nexus Expression, PANTHER [31], DAVID [32], and Gene Set Enrichment Analysis (GSEA) software [33]. Differentially expressed genes and CNAs were integrated with Nexus Copy Number. The microarray data are available from the Gene Expression Omnibus (GEO) database (https://ncbi.nlm.nih.gov/geo/, Accession No. GSE153002).

RT-qPCR analyses of ACC tumor tissue ($n = 30$) and cultured, low-passage ACC cells used TaqMan gene expression assays (Thermo Fisher Scientific, Waltham, MA, USA) for *DFFA* (Hs00189336_m1), *DFFB* (Hs00237077_m1), *GUSB* (Hs00939627_m1), *KIF1B* (Hs01114511_m1), *MFN2* (Hs00208382_m1), *PARK2* (Hs00247755_m1), *TP73* (Hs01056230_m1), and *UBC* (Hs01871556_s1). Relative expression levels were calculated by the ddCT method [34].

Sphere, proliferation, adhesion, and apoptosis assays

Cultured ACC cells were derived from ACC67 (grade 1) [13] and ACC100 (grade 3) (supplementary material, Table S1). Both tumors were *MYB::NFIB* fusion positive. In addition, ACC67 showed gain of 19p13.11-pter as the only copy number change, whereas ACC100 had 17 different gains and losses, including loss of 1p36 and *PARK2* (6q26). Low-passage, mycoplasma-free cells were used and validated for *MYB::NFIB* fusion transcripts, as described [13]. Cells were transfected with 50 nM Silencer Select siRNAs for *KIF1B* (s23022, s23024), *MFN2* (s19261, s19262), *PARK2* (s10043, s10044), *TP73* (s14320, s14321), or negative control siRNAs using the Lipofectamine RNAiMAX transfection reagent (Thermo Fisher Scientific) [13]. For sphere assays, cells were grown for 10 days under nonadherent conditions in six-well plates precoated with PolyHEMA (Merck, Darmstadt, Germany), as described [35]. For proliferation assays, two million cells were seeded in T25 flasks and counted 7 days later using a Countess 3 cell automated counter (Thermo Fisher Scientific). Alternatively, 400,000 cells were seeded in six-well plates and grown for 48 h. Cells were supplemented with 10 μM BrdU during the last 16 h and subsequently fixed and stained using a FITC BrdU Flow kit (Becton, Dickinson and Company, BD, Franklin Lakes, NJ, USA). Stained cells were analyzed with the Accuri C6 flow cytometer (BD). Cell adhesion was evaluated in 96-well plates precoated with collagen type I solution (Merck). Twenty thousand cells were allowed to adhere overnight and then treated with 0.25% Trypsin–EDTA solution (Thermo Fisher Scientific) for 2.5 min. The relative number of remaining adherent cells was estimated with the Alamar Blue reagent (Thermo Fisher Scientific). For apoptosis assays, cells were seeded in 96-well plates (BD) and treated with 50 nM siRNAs for 96 h followed by 1 μM doxorubicin, vinorelbine, palbociclib, or AZD4573 (Selleck Chemicals, Houston, TX, USA) for 24 h and analyzed with the Caspase-Glo 3/7 reagent (Promega, Madison, WI, USA) [14]. Cellular protein expression was analyzed by immunoblotting using mouse monoclonal antibodies to PARK2 (mAb 4211, Cell Signaling Technology, Danvers, MA, USA) and beta-actin (ab8226, Abcam, Cambridge, UK) [13]. Live tumor cells were imaged with a Zeiss Axiovert A1 microscope equipped with an AxioCam ERc5s camera and cell size was measured using a Countess 3 cell automated counter (Thermo Fisher Scientific).

Statistical analyses

Associations between CNAs and clinicopathological parameters as well as the fraction of downregulated genes within the 1p36 deletion compared with the copy number neutral chromosome 13 were analyzed using a χ^2 test. Overall survival (OS) was defined as the time from initial diagnosis to death (any cause) or last follow-up. Survival was estimated using Kaplan–Meier tests, and differences between groups were analyzed with the log-rank test. The hazard function of death was estimated by Cox regression. Multivariate analyses were adjusted for 1p36 deletion, age at diagnosis, stage, and tumor grade. Confirmation of the proportional hazards assumption and linearity of Martingale and deviance residuals was done with the survival package in R. Median survival as a function of 1p36 deletion and age at diagnosis was estimated with Poisson regression. Differences in gene expression in patient samples measured by RT-qPCR were evaluated using nonparametric Mann–Whitney tests. Significant differences between groups were assessed by one-way ANOVA or independent samples t-test. Prism version 9 (Graphpad, La Jolla, CA, USA),

SAS version 9.3 (SAS Institute, Cary, NC, USA), SPSS Statistics version 28 (IBM, Armonk, NY, USA), and R (https://www.r-project.org) were used for statistical analyses; $p < 0.05$ was considered statistically significant.

Results

The landscape of CNAs in ACC

Analysis of 100 ACC patient samples by arrayCGH revealed 527 CNAs, including 392 focal and 135 whole-chromosome-/arm-level changes (Figure 1A,B; supplementary material, Table S1). There was no statistical difference between the number of CNAs in the previously published 40 ACCs [25] and the 60 new cases in this study ($p = 0.56$), validating our new extended results (supplementary material, Figure S2A). Moreover, there were no statistical differences in the number of CNAs or 1p and 6q deletions between FFPE and fresh frozen tissues (supplementary material, Figure S2B–D). CNAs were more abundant in tumors with solid histology (grade 3) than in tumors with tubular and cribriform histologies (grades 1 and 2) ($p < 0.0001$; Figure 1A). Sixty-six percent of the patients had five or fewer CNAs/tumor (supplementary material, Figure S3) and survived longer than patients with ≥6 CNAs/tumor ($p = 0.037$) (Figure 1C).

Nineteen recurrent CNAs were identified (supplementary material, Table S3). The most common losses were 12q13.13 (27%), 6q25.1–q25.3 (26%), 6q25.3–q26 (26%), 1p36.32–p36.12 (17%), and 14q23.2–q24.3 (14%). The most common gains were 9p23–p22.3 (18%), 9p24.3–p23 (13%), 19q13.13–q13.32 (13%), and 19q13.32–q13.42 (13%).

GISTIC2.0 identified four regions of significant focal CNAs ($Q < 0.05$) across the ACC genome, including losses of 1p36.32–p36.21, 6q25.1–q27, 9p24.3–p23, and 12q13.13–q13.2 (Figure 1B). Peak regions containing single genes were also identified in 6q26 (*PARK2*, a.k.a. *PRKN*) and 12q13.13 (*SLC11A2*) (supplementary material, Table S4). Deletions involving *PARK2* were found in 28% of cases (Figure 1D), including one with an intragenic deletion. OS was shorter among patients with 1p36 ($p < 0.0001$) or *PARK2* ($p = 0.0042$) deletions than among those without such deletions (supplementary material, Figure S4A,B). Conversely, OS did not differ between patients with and without 9p or 12q deletions (data not shown).

Genomic imbalances with breakpoints in or immediately distal to *MYB* were detected in 16% of ACCs. Two tumors had interstitial deletions within 1 Mb telomeric to *MYB*, and one had an interstitial deletion 0.59 Mb centromeric to *MYB*. Four tumors showed gain of one *MYB* allele (supplementary material, Figure S5).

Concurrent loss of 1p36.32–p36.21 and 6q23.3–qter ($p = 0.03$) (Figure 1E) was only seen in ACCs with solid histology. Loss of 1p36.32–p36.21 was also associated with gains of 1p34.3–q41 ($p = 0.003$), 6p25.3–q23.3 ($p = 0.006$), 8p23.3–q24.3 ($p = 0.0007$), and 9p24.3–p23 ($p = 0.02$) and with losses of 11p15.5–p11.2 ($p = 0.003$) and 17p13.1–p12 ($p = 0.01$) (Figure 1E). Loss of 6q23.3–qter was associated with gain of 9pter–p22.3 ($p = 0.008$) and loss of 1p36.32–p36.22 ($p = 0.028$) (Figure 1F).

Eighteen focal amplifications were identified in six tumors (supplementary material, Table S5 and Figure S5). Amplifications of *KIT* and *PDGFRA* were identified in two cases, high-level amplification of *MYB* in one case, and amplifications of *HMGA2* and *MDM2* in one. Homozygous deletion of *CDKN2A/B* and a chromothrypsis-like event in 12p11.23–q23.3 were seen in one case each (supplementary material, Table S5).

PARK2 is a putative tumor suppressor gene in ACC

GISTIC2.0 identified a peak region in 6q25.3–q26, containing *PARK2* as the only gene (Figure 1B,D). RT-qPCR analysis of 30 ACCs revealed that *PARK2* expression was significantly lower in tumors with 6q deletions than in those without (Figure 1G). ACC cells with 6q/*PARK2* deletion (ACC100) showed significantly higher sphere formation compared with ACC cells without deletion (ACC67) (Figure 2A). To investigate whether decreased levels of PARK2 affected the spherogenesis of ACC cells, we knocked down *PARK2* expression in cultured ACC cells without 6q deletion. RT-qPCR and western blot analyses revealed robust knockdown of *PARK2* mRNA and protein levels in ACC67 cells (Figure 2B), whereas *PARK2* mRNA and protein expression were not repeatedly detected or were undetected in ACC100 cells. PARK2 downregulation led to a two- to three-fold increase in the formation of ACC tumor spheres under anchorage-independent growth conditions (Figure 2C). Notably, ACC cells with *PARK2* deletion showed decreased apoptosis in response to doxorubicin treatment compared to cells without *PARK2* deletion (Figure 2D). This is further supported by studies showing that PARK2 knockdown leads to decreased apoptosis in response to doxorubicin treatment (Figure 2E). Taken together, our findings suggest that *PARK2* has tumor suppressor activity with effects on both tumor growth and resistance to therapy in ACC.

Molecular consequences of 1p36 deletion

To study the molecular consequences of 1p36 deletions, we analyzed the mRNA expression of genes located within 1p36.32–p36.21 (GISTIC2.0 region) in 30 tumors with ($n = 10$) and without ($n = 20$) 1p36 deletion. Twenty-seven of the 128 genes in this segment were significantly downregulated in tumors with 1p36 deletion ($p < 0.05$) (Figure 2F) (supplementary material, Table S6), which is significantly more than expected ($p < 0.0001$). These results were confirmed by GSEA (Figure 2G). In a gene ontology analysis, apoptosis and

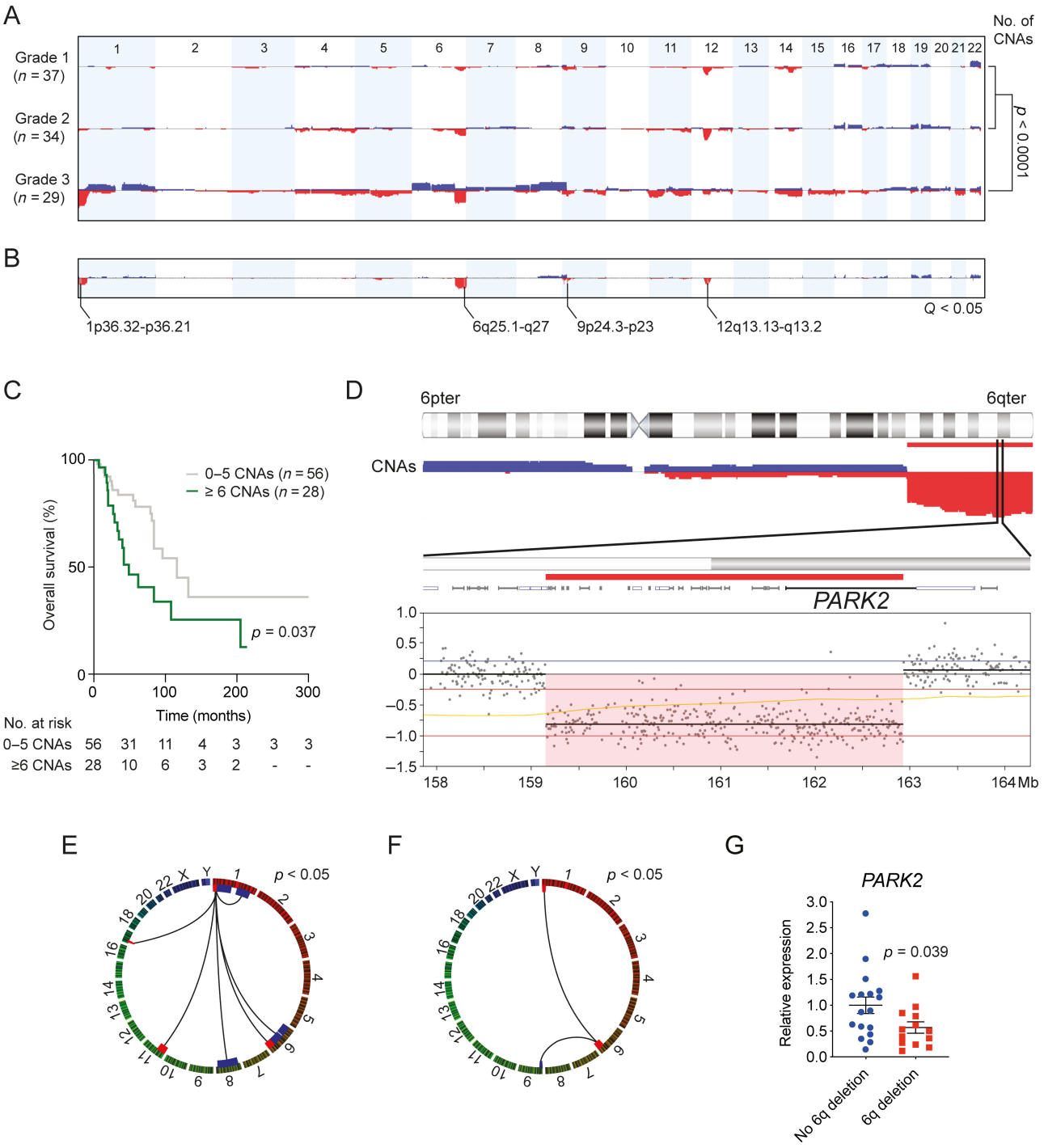

Figure 1. Genomic profiling of 100 ACCs. (A) Genome-wide plots showing distribution of CNAs in grades 1, 2, and 3 tumors. CNAs were significantly more abundant in grade 3 tumors (solid histology) than in grades 1 and 2 tumors (tubular and cribriform histologies). Note that 1p36 deletions were found almost exclusively in grade 3 tumors (χ^2 test). (B) GISTIC2.0 identified four regions of significant focal CNAs ($Q < 0.05$) across the ACC genome. (C) Kaplan–Meier curves showing that patients with ≥6 CNAs/tumor had a significantly shorter OS than those with ≤5 CNAs/tumor (log-rank test). (D) Distribution of 6q deletions (red) detected by arrayCGH in 100 ACCs. Deletion of almost the entire *PARK2* gene (exons 2–12) and flanking centromeric sequences in ACC76. (E and F) Circos plots showing gains (blue) and losses (red) co-occurring with deletions involving 1p36.32–p36.12 (E) and 6q25.1–q26 (F). (G) RT-qPCR analysis of *PARK2* expression in surgical specimens of 30 ACCs with and without deletion of *PARK2* (Mann–Whitney test).

the pentose-phosphate shunt were significantly enriched biological processes associated with the downregulated genes in 1p36 (Figure 2H). RT-qPCR analysis confirmed that the pro-apoptotic genes *TP73*, *MFN2*, *KIF1B*, *DFFA*, and *DFFB* in 1p36 were significantly downregulated in tumors with 1p36 deletion (Figure 2I), suggesting that the copy number losses in 1p36 are associated with resistance to apoptosis. To test this hypothesis, we transfected cultured ACC cells from two cases (ACC67 and ACC100) with individual siRNAs targeting the early pro-apoptotic genes *TP73*, *MFN2*, and *KIF1B* for 5 days (Figure 2J). We also

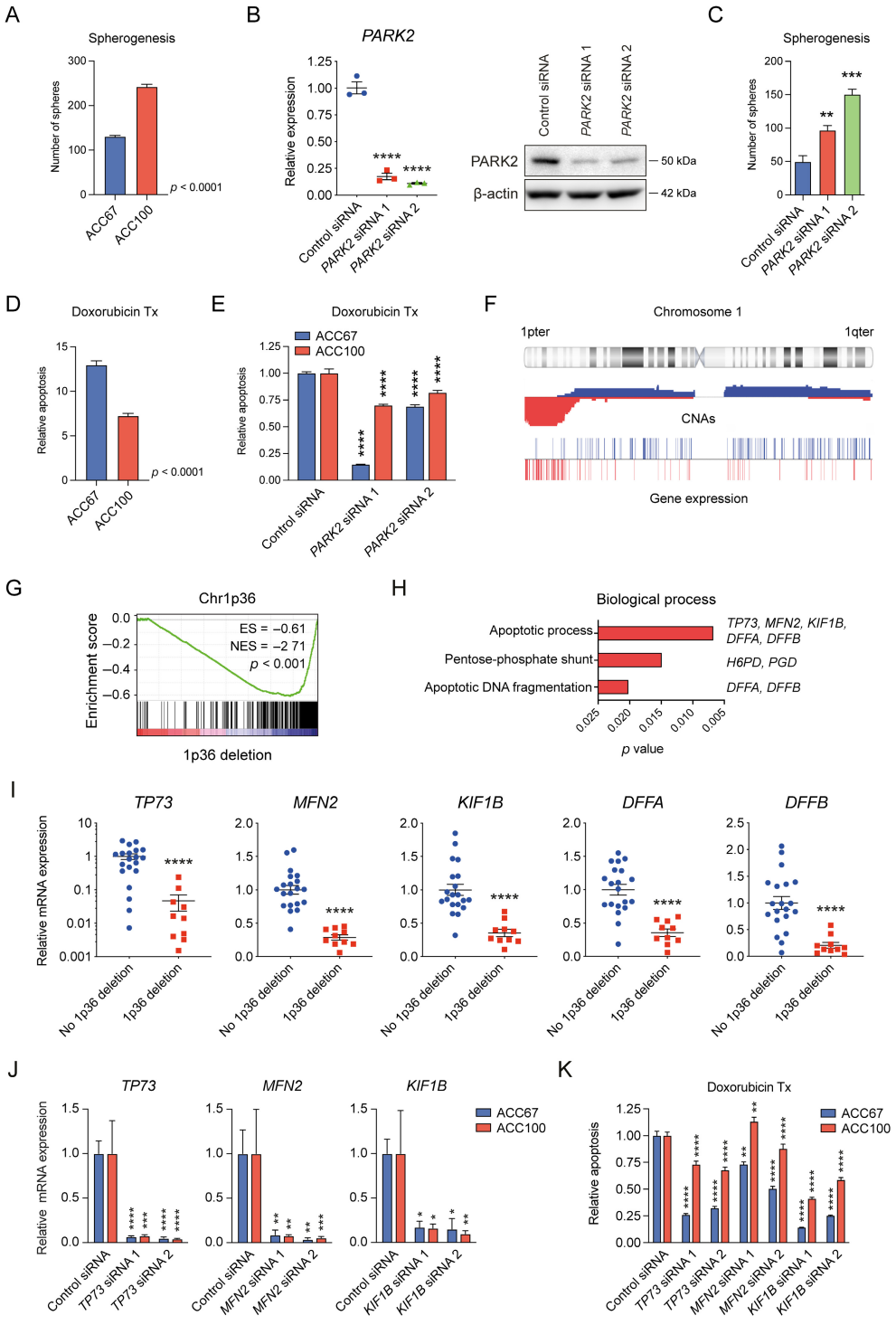

Figure 2. Molecular and functional consequences of *PARK2* and 1p36 deletions in ACC. (A) Spherogenesis in ACC100 cells with *PARK2* and 1p36 deletions and in ACC67 cells without these deletions. Cells were cultured under nonadherent conditions for 10 days. Data show the average of three independent experiments. (B) RT-qPCR and western blot analyses of *PARK2* mRNA and protein expression in ACC cells after treatment with 50 nM *PARK2* siRNAs for 48 h. (C) Sphere formation 10 days after *PARK2* knockdown in ACC cells. Experiments were done three times with six biological replicates. (D) ACC100 cells are less sensitive to doxorubicin treatment (1 μM, 24 h) compared to ACC67 cells. (E) Knockdown of *PARK2* decreases apoptosis (caspase 3/7 activity) in cultured ACC cells after 24 h treatment with 1 μM doxorubicin. Data represent one of three independent experiments with five biological replicates. (F) Distribution of 1p deletions (red) detected by arrayCGH in 100 ACCs. The lower panel shows the expression of differentially expressed genes in tumors with and without 1p deletions. Underexpressed genes are indicated in red. (G) GSEA showing enrichment of downregulated genes in a publicly available 1p36 gene set in ACCs with 1p36 deletion. (H) Gene Ontology analysis of genes downregulated in 1p36 in tumors with 1p36 deletion. (I) RT-qPCR analysis of pro-apoptotic genes located in 1p36 in ACCs with ($n = 10$) or without ($n = 20$) 1p36 deletion (Mann–Whitney test). (J) Knockdown of pro-apoptotic genes *TP73*, *MFN2*, and *KIF1B* in ACC67 and ACC100 cells. Data show one of three independent experiments with three biological replicates. (K) Knockdown of 1p36 genes decreases apoptosis (caspase 3/7 activity) in cultured ACC cells after treatment with doxorubicin. Results shown represent one of three independent experiments with five biological replicates. Mean ± SEM. $^{**}p < 0.01$, $^{***}p < 0.001$, $^{****}p < 0.0001$ by independent sample *t*-test or one-way ANOVA.

treated siRNA-transfected cells with doxorubicin or vinorelbine during the last 24 h and measured caspase 3/7 activity. Downregulation of any of the three genes significantly decreased apoptosis induced by these chemotherapeutic drugs, though the effect was weaker for *MFN2* and only significant with one siRNA for each case (Figure 2K; supplementary material, Figure S6A–C). Thus, deletion of *TP73* and *KIF1B* promotes resistance to apoptosis in ACC cells.

Next, we compared the mutation frequency of genes in 1p36.32–p36.21 with that of all genes in 83 sequenced ACCs in The Cancer Genome Atlas (TCGA) [16,17]. We found no significant difference ($p = 0.55$); only four nonrecurrent mutations were identified in genes in this region, and only one tumor had a 1p36 deletion. Evidently, 1p36 deletions result in a gene dosage effect and downregulation of several pro-apoptotic genes, rendering ACCs with 1p36 deletions resistant to apoptosis.

Deletions of 1p36 and PARK2 correlate with survival and tumor grade

To further validate the significance of 1p36 and *PARK2* deletions, we studied their frequency by FISH in an independent large cohort of ACCs. Deletions of 1p36 were found in 13.5% of the cases (53/392 analyzable cases showed loss of one or both 1p36 probe signals) and loss of one *PARK2* allele in 24.3% (59/243 analyzable cases) (Figure 3A,B).

To evaluate the clinical significance of the 1p36 and *PARK2* deletions, we studied the correlation between these aberrations and various clinicopathological parameters in our ACC cohort (supplementary material, Table S7). Survival analyses revealed significantly shorter OS in patients with 1p36 deletions than in those without ($p < 0.0001$) (Figure 4A); patients with 1p36 deletions also had shorter median survival (38 versus 147 months; 95% CI 34–42 and 110–184, respectively) and shorter 5-year OS (27% versus 77%). Patients with *PARK2* deletions also had shorter OS than those without ($p = 0.0008$) (Figure 4B). Notably, patients with concurrent deletions of 1p36 and *PARK2* had shorter OS than patients with either one or neither of these deletions ($p < 0.0001$) (Figure 4C).

Next, we estimated the hazard function of death of ACC patients with Cox regression. In univariate analysis, the hazard function was significantly dependent on 1p36 deletion, *PARK2* deletion, age at diagnosis, stage III and IV, and tumor grade 3 (supplementary material, Table S8). In multivariate analysis, the significant risk factors of death were 1p36 deletion, age, stage III and IV, and tumor grade 3. Median survival of patients with or without 1p36 deletion calculated with the hazard function also revealed that the effect of 1p36 deletion on survival is dependent on the age of the patient at diagnosis (Figure 4D). At 53 years of age (the median age at diagnosis in our study), a patient with a 1p36 deletion has an expected survival of less than 5 years versus ~15 years in a patient without the deletion.

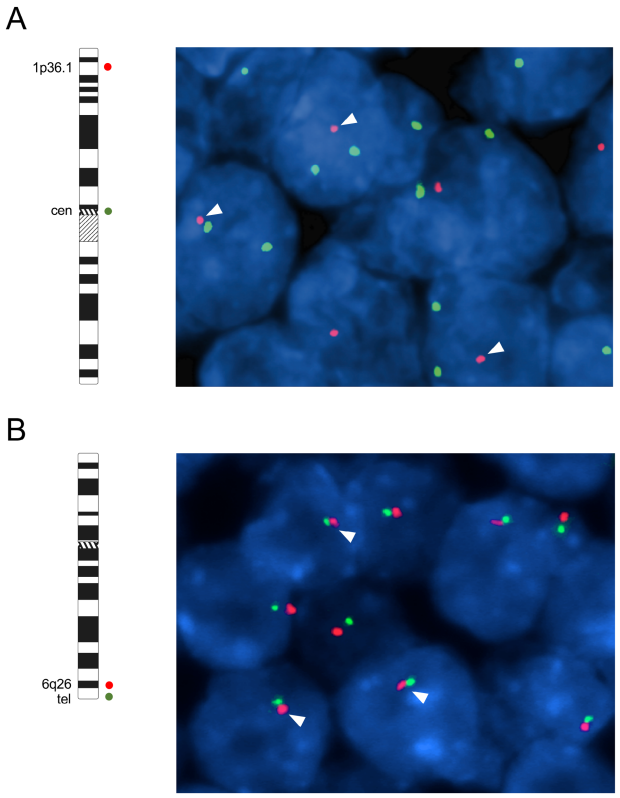

Figure 3. FISH analyses of 1p36 and *PARK2* gene deletions in ACC. (A) ACC with deletion in 1p36, shown by loss of one *KLHDC7A* (1p36.13) red signal and retention of two green signals from the centromere probe. Arrowheads indicate retained *KLHDC7A* allele. (B) ACC with loss of one copy each of *PARK2* (6q26) and 6q subtelomeric region, shown by loss of one red and one green signal. Arrowheads indicate remaining intact copy of *PARK2* and 6q subtelomeric region (red/green signals). Nuclei are stained in blue with DAPI. Ideograms of chromosomes 1 and 6 with the location of the FISH probes used are shown to the left of each FISH image.

Deletions of 1p36 were overrepresented in tumors with solid histology ($p < 0.0001$) (Figure 4E), as were deletions of *PARK2* ($p = 0.002$) (data not shown) and deletions of both 1p36 and *PARK2* ($p < 0.0001$) (Figure 4F). Cox regression analysis of grade 3 tumors only ($n = 63$) revealed that 1p36 deletion ($p = 0.01$) and *PARK2* deletion ($p < 0.001$) predicted shorter OS in this select subgroup. Furthermore, the risk of death in patients having 1p36 deletion was similar between different tumor grades, whereas it was increased in grade 3 tumors with *PARK2* deletion ($p = 0.005$). These results indicate that 1p36 deletion predicts shorter OS regardless of tumor grade, whereas *PARK2* deletion confers an additional risk in high-grade tumors. Collectively, these findings show that 1p36 and *PARK2* deletions are recurrent prognostic biomarkers in ACC and that 1p36 deletion is an independent predictor of OS in multivariate analysis.

A gene expression signature that defines a subset of ACC with 1p36 deletion and short OS

To study the effect of genomic alterations on gene expression, we performed unsupervised hierarchical clustering and principal component analysis of global

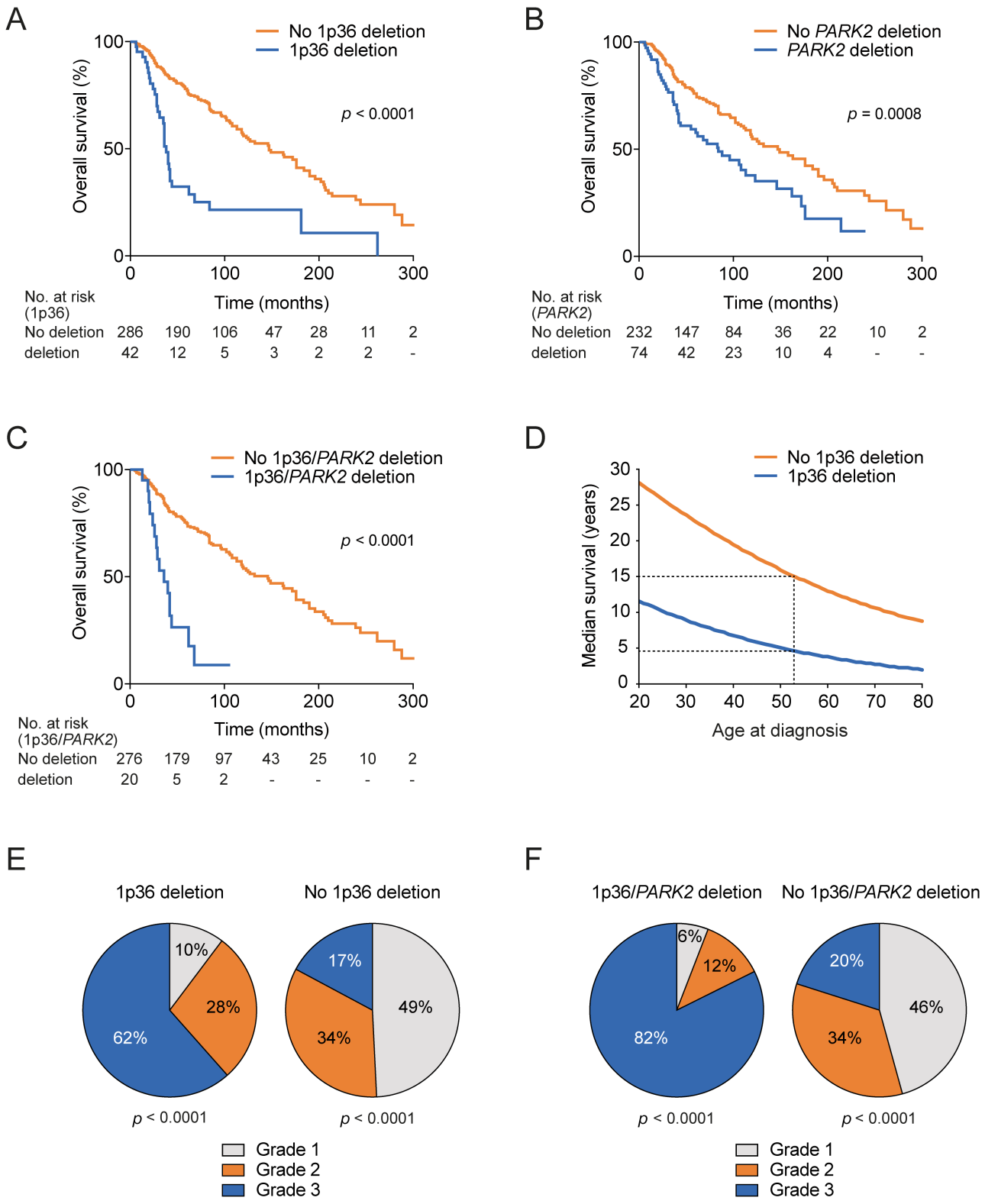

Figure 4. OS of ACC patients with 1p36 and/or *PARK2* deletions. (A) 1p36 deletion versus no 1p36 deletion (log-rank test). (B) *PARK2* deletion versus no *PARK2* deletion (log-rank test). (C) 1p36 and *PARK2* deletions versus no 1p36 and *PARK2* deletions (log-rank test). (D) The effect of 1p36 deletion on survival is significantly dependent on patient age at diagnosis. Dashed lines indicate median survival for 53-year-old ACC patients (median age of the patients in this investigation) with and without 1p36 deletion. (E and F) Pie charts show significant overrepresentation of 1p36 deletions (E) and of concurrent 1p36 and *PARK2* deletions (F) in grade 3 ACCs (χ^2 test).

gene expression data from 30 ACCs with known genomic profiles. The ACCs formed two major clusters – designated ACC-I and ACC-II – that were clearly separated from NSG (Figure 5A,B). *MYB* or *MYBL1* was activated in all tumors in both clusters (supplementary material, Figure S7).

Tumors in the ACC-I cluster had markedly more CNAs than those in the ACC-II cluster (Figure 5C).

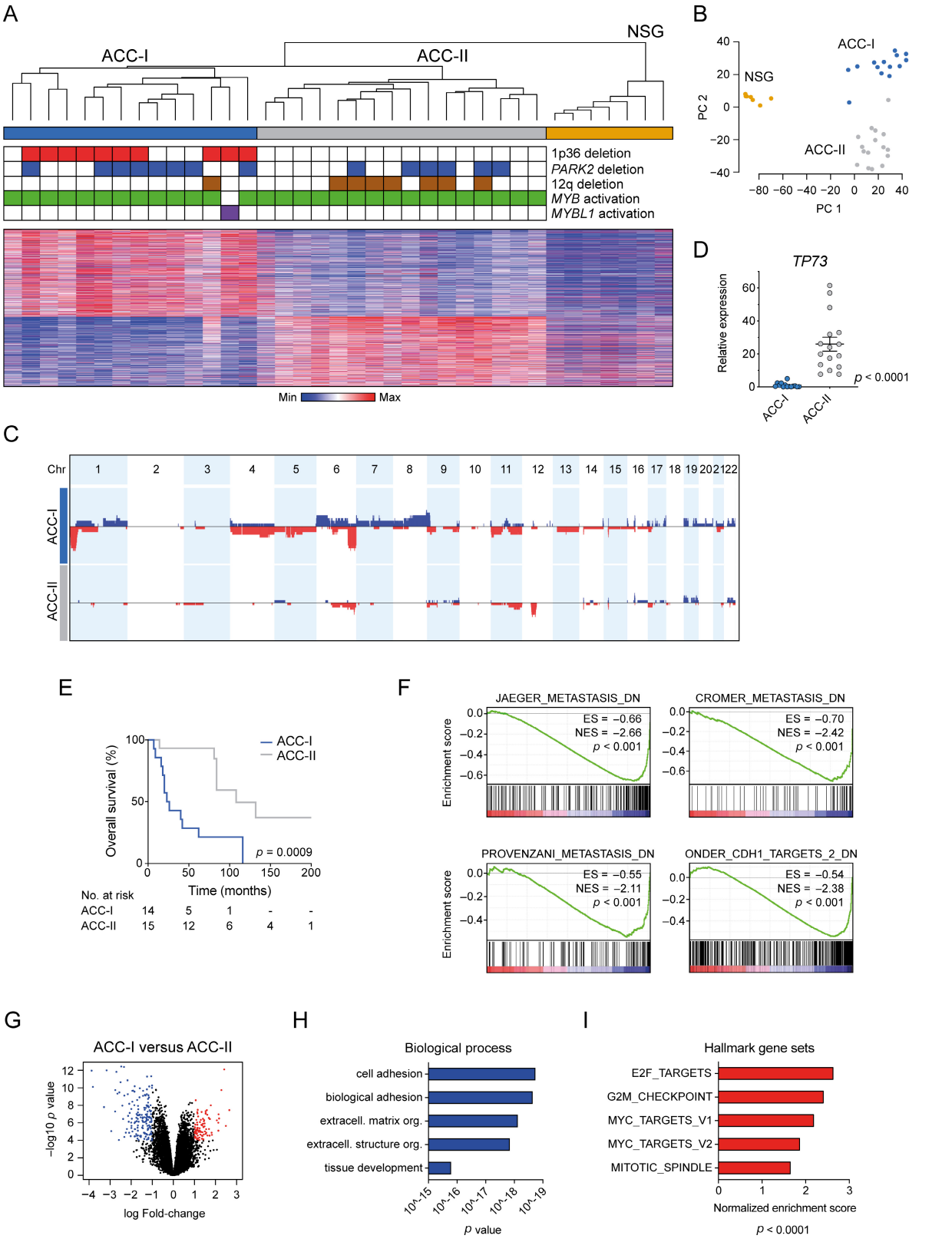

Figure 5. Global gene expression analysis identifies two clusters of ACC with significantly different copy number profiles and patient survival. (A) Unsupervised hierarchical clustering and heatmap analysis of global gene expression in 30 ACCs and 7 NSGs. The presence or absence of deletions of 1p36, *PARK2*, and 12q and the *MYB/MYBL1* status are indicated. (B) Principal component analysis of global gene expression in 30 ACCs and seven NSGs. (C) CNAs in tumors in ACC-I and ACC-II clusters. (D) RT-qPCR analysis of 30 ACC surgical specimens showing significantly lower *TP73* expression in ACC-I tumors than in ACC-II tumors. Mean ± SEM (Mann–Whitney test). (E) Kaplan–Meier survival analysis of patients in ACC-I and ACC-II clusters (log-rank test). (F) GSEA of tumors with and without 1p36 deletion. (G) Volcano plot showing most significantly upregulated (red) and downregulated (blue) genes in ACC-I versus ACC-II cluster. (H) Gene Ontology analysis of genes downregulated in ACC-I versus ACC-II tumors. (I) GSEA of global gene expression showing enrichment of Hallmark gene sets in ACC-I versus ACC-II tumors.

Deletions of 1p36 were found exclusively in ACC-I tumors, and *PARK2* deletions were more frequent in ACC-I tumors (Figure 5A,C). Gains of 6p and 8q were found only in ACC-I tumors (Figure 5C). In contrast, all but one of the tumors with 12q deletions were in the ACC-II cluster. ACC-I tumors, including four lacking 1p36 deletions, had significantly lower expression of the pro-apoptotic gene *TP73* than ACC-II tumors (Figures 2I and 5D). Importantly, OS was markedly shorter in patients with ACC-I tumors (Figure 5E). Thus, the gene expression and copy number profiles are significantly associated with the prognosis of ACC.

To investigate the biological processes associated with the expression profiles of the two clusters, we used GSEA. Gene sets downregulated in invasive and metastatic tumors were significantly associated with ACC-I tumors (Figure 5F). In global gene expression and gene ontology analyses, the most significantly downregulated genes (163 genes, $p < 0.0001$) in the ACC-I versus ACC-II cluster (Figure 5G) were involved in cell adhesion and extracellular matrix organization (Figure 5H). Expression of genes involved in cell proliferation (e.g., *MKI67*; $p = 0.002$) was higher in ACC-I than in ACC-II tumors (Figure 5I), suggesting that ACC-I tumors grow faster and are more prone to metastasize than ACC-II tumors.

Next, we studied cellular characteristics of cultured ACC cells with (ACC100) and without (ACC67) 1p36 and *PARK2* deletions. ACC cells with 1p36/*PARK2* deletions had a higher proliferation rate and reduced surface adhesion compared to cells without deletions (supplementary material, Figure S8A–C). Moreover, ACC cells with 1p36/*PARK2* deletions had a smaller size, grew in multilayers, and had a less prominent cytoplasm (supplementary material, Figure S8D,E). Both ACC cells with and without 1p36/*PARK2* deletions were resistant to treatment with the CDK4/6 inhibitor palbociclib (supplementary material, Figure S8F). However, cells with these deletions were sensitive to the CDK9 inhibitor AZD4573 (supplementary material, Figure S8G), and knockdown of *TP73*, *KIF1B*, and *PARK2* reduced the apoptotic response induced by this drug (supplementary material, Figure S8H).

Discussion

A major challenge in the management of ACC patients is the high rate of recurrences and distant metastases and the lack of effective systemic therapies and clinically useful prognostic biomarkers. Using an integrated genomic and transcriptomic approach, we now demonstrate that deletions of 1p36 and *PARK2* are significant prognostic biomarkers in ACC and that loss of pro-apoptotic genes in 1p36 and loss of the tumor suppressor *PARK2* contribute to aggressive behavior and poor survival in ACC.

Our analyses identified losses involving 1p36, 6q (*PARK2*), 9p, and 12q as significant focal CNAs in ACC. OS was significantly shorter in patients with 1p36 or *PARK2* deletions than in those without such deletions. This observation was further validated by FISH in a large cohort of ACC patients with clinical follow-up. The 1p36 deletion independently predicted short OS on multivariate analysis consistent with the results of smaller studies of ACC [36,37]. Interestingly, we also found that the effect of the 1p36 deletion on survival was dependent on patient age at diagnosis. Finally, we showed that concurrent deletions involving 1p36 and *PARK2* were associated with the shortest OS and preferentially occurred in poorly differentiated (grade 3) ACCs. We anticipate that these prognostic biomarkers will be clinically useful for treatment selection and for stratification of patients in clinical trials and that in a clinical setting they are best analyzed by FISH using robust 1p36 and *PARK2* probes. Future studies will show whether immunohistochemistry for PARK2 and/or tumor suppressor proteins encoded by genes in 1p36 (e.g., TP73) will be feasible.

The clinical consequences of 1p36 deletions in ACC prompted us to investigate their molecular underpinnings. Gene expression profiling revealed downregulation of a significant number of genes in 1p36 in ACCs with deletions. Further analysis identified apoptosis as a significantly inhibited pathway in tumors with 1p36 deletions. RT-qPCR confirmed downregulation of several pro-apoptotic genes, including the early genes *TP73*, *KIF1B*, and *MFN2* [38–41]. Consistent with previous observations in other tumors [42], we found evidence of monoallelic expression of *TP73* in ACC since tumors with loss of one copy of 1p36 had much lower, or almost undetectable, levels of *TP73* than tumors without deletions. Reduced expression of pro-apoptotic genes in 1p36 as a result of haploinsufficiency may lead to inhibition of stress-induced apoptosis and resistance to cytotoxic therapies. Indeed, knockdown of in particular *TP73* and *KIF1B* in ACC cells without 1p36 deletions increased resistance to apoptosis induced by cytostatic drugs. In summary, we identified the pro-apoptotic genes *TP73* and *KIF1B* as potential 1p36 tumor suppressor genes in ACC. Reduced expression of these genes as shown by copy number loss was associated with poor survival and increased resistance to apoptosis. Previous studies of ACC failed to detect any recurrent mutations in genes in 1p36 [16,23], supporting the notion that the major molecular consequences of the 1p36 deletions are dosage-dependent impairment of multiple genes in this region. This conclusion is also consistent with studies of other cancer types with recurrent copy number losses in 1p36 [43–45].

Copy number profiling identified the tumor suppressor gene *PARK2* [46–48] as a single candidate target gene of the 6q deletions in ACC. Expression analysis confirmed that *PARK2* expression is indeed lower in ACCs with 6q26 deletions than in those without. Moreover, *PARK2* knockdown in ACC cells without 6q26 deletions increased spherogenesis and decreased apoptosis in response to chemotherapeutic drugs. Thus, *PARK2* loss increases tumor growth initiated by ACC stem/progenitor cells and increases resistance to apoptosis. *PARK2* encodes the E3 ubiquitin ligase Parkin

[49,50] and is an important cell-cycle regulator and a master regulator of G1/S cyclins [51]. PARK2 also regulates apoptosis through BCL-XL [52], and loss of PARK2 function can activate PI3K/AKT signaling through inactivation of PTEN [53]. The *PARK2* tumor suppressor is mutated, or more commonly deleted and downregulated, in for example, lung cancer, glioblastoma, colon cancer, ovarian cancer, and melanoma [46–48,54–56]. Our findings suggest that *PARK2* is also a tumor suppressor in ACC that is associated with poor prognosis in a subset of tumors. This observation is further supported by our recent study showing that losses of sequences distal to the *MYB* locus in 6q23.3 preferentially occur in grade 3 tumors and are associated with poor OS in ACC [24].

Integrated transcriptomic and copy number profiling revealed several previously unrecognized events associated with ACC tumorigenesis. Unsupervised cluster analysis identified two major clusters of ACCs that differed in genomic profile and clinical outcome. Tumors in the ACC-I cluster had 1p36 deletions, multiple CNAs, and gains of 6p and 8q, whereas tumors in the ACC-II cluster lacked these aberrations, had fewer CNAs, and preferentially had 12q deletions. Although present in both clusters, *PARK2* deletions were more frequent in the ACC-I cluster. Importantly, patients in this cluster also had a significantly shorter OS. Similar groups with different expression profiles and prognosis have previously been identified in transcriptomic studies of ACCs [57,58]. In the present study, the transcriptomic profiles of ACC-I tumors were associated with increased cell proliferation, invasion, and metastasis, consistent with the aggressiveness of these tumors. Collectively, our results identified a gene expression signature associated with short OS, multiple CNAs including 1p36 deletions, and reduced expression of *TP73*.

A limitation of our study is the paucity of functional studies of the candidate tumor suppressor genes in 1p36 and distal 6q, mainly reflecting the lack of authentic ACC cell lines and the difficulty of culturing ACC cells *in vitro* [13,59]. Another limitation is that extensive mutational data were not available for our patient cohort. On the other hand, the comprehensive genomic data from 366 ACC patients with clinical follow-up enabled us to identify reliable prognostic biomarkers for ACC.

In summary, we used an integrated copy number and transcriptomic approach to identify novel driver genes and prognostic biomarkers in ACC. We found that copy number losses of 1p36 and *PARK2* are potential prognostic biomarkers in ACC and that loss of pro-apoptotic genes in 1p36 and loss of the tumor suppressor *PARK2* contribute to aggressive behavior and short OS in ACC. Our findings provide new important insights into the pathogenesis of ACC that have implications for biomarker-driven stratification of patients in clinical trials.

Acknowledgements

We thank Prof. Dr. med. Guido Sauter and PD Dr. med. Waldemar Wilczak at the Institute for Pathology, University Medical Center Hamburg-Eppendorf, for generously providing FFPE sections from tissue microarrays containing well-characterized ACCs. We also thank Dr. Junchi Huang for valuable technical assistance, Prof. Anders Odén for statistical analyses, and the SciBlu Genomics Facility at Lund University for microarray service. This study was supported by grants from the Swedish Cancer Society, the Swedish state under an agreement between the Swedish government and country councils, the ALF agreement (ALFGBG-721711), the Adenoid Cystic Carcinoma Research Foundation (ACCRF), the AG Fund, and the Royal Society of Arts and Sciences in Gothenburg.

Author contributions statement

GS, MP and MKA designed and supervised the study. PES, YM, AKE-N, MSB-W, HFF, CM, IF, RF, WB, TL and GS collected and processed tissue samples and clinical data and reviewed the histopathological diagnoses. MP, MKA and GS generated and analyzed the experimental data and performed bioinformatic and statistical analyses. GS, MP and MKA drafted the manuscript. All authors reviewed, edited, and approved the final version of the manuscript.

Data availability statement

The arrayCGH data and gene expression microarray data are available for download from the Gene Expression Omnibus database (https://ncbi.nlm.nih.gov/geo/, Accession Nos. GSE153228 and GSE153002).

References

1. Stenman G, Licitra L, Said-Al-Naief N, *et al*. Adenoid cystic carcinoma. In *World Health Organization Classification of Head and Neck Tumours*, El-Naggar AK, Chan JKC, Grandis JR, *et al*. (eds). IARC Press: Lyon, 2017; 164–165.
2. Brill LB 2nd, Kanner WA, Fehr A, *et al*. Analysis of MYB expression and MYB-NFIB gene fusions in adenoid cystic carcinoma and other salivary neoplasms. *Mod Pathol* 2011; **24:** 1169–1176.
3. Laurie SA, Ho AL, Fury MG, *et al*. Systemic therapy in the management of metastatic or locally recurrent adenoid cystic carcinoma of the salivary glands: a systematic review. *Lancet Oncol* 2011; **12:** 815–824.
4. Carlson J, Licitra L, Locati L, *et al*. Salivary gland cancer: an update on present and emerging therapies. *Am Soc Clin Oncol Educ Book* 2013; **33:** 257–263.
5. Coca-Pelaz A, Rodrigo JP, Bradley PJ, *et al*. Adenoid cystic carcinoma of the head and neck–an update. *Oral Oncol* 2015; **51:** 652–661.
6. Xu B, Drill E, Ho A, *et al*. Predictors of outcome in adenoid cystic carcinoma of salivary glands: a clinicopathologic study with correlation between MYB fusion and protein expression. *Am J Surg Pathol* 2017; **41:** 1422–1432.
7. Stenman G, Sandros J, Dahlenfors R, *et al*. 6q- and loss of the Y chromosome–two common deviations in malignant human salivary gland tumors. *Cancer Genet Cytogenet* 1986; **22:** 283–293.

8. Nordkvist A, Mark J, Gustafsson H, *et al*. Non-random chromosome rearrangements in adenoid cystic carcinoma of the salivary glands. *Genes Chromosomes Cancer* 1994; **10:** 115–121.
9. Persson M, Andrén Y, Mark J, *et al*. Recurrent fusion of MYB and NFIB transcription factor genes in carcinomas of the breast and head and neck. *Proc Natl Acad Sci U S A* 2009; **106:** 18740–18744.
10. Mitani Y, Liu B, Rao PH, *et al*. Novel MYBL1 gene rearrangements with recurrent MYBL1-NFIB fusions in salivary adenoid cystic carcinomas lacking t(6;9) translocations. *Clin Cancer Res* 2016; **22:** 725–733.
11. Brayer KJ, Frerich CA, Kang H, *et al*. Recurrent fusions in MYB and MYBL1 define a common, transcription factor-driven oncogenic pathway in salivary gland adenoid cystic carcinoma. *Cancer Discov* 2016; **6:** 176–187.
12. Drier Y, Cotton MJ, Williamson KE, *et al*. An oncogenic MYB feedback loop drives alternate cell fates in adenoid cystic carcinoma. *Nat Genet* 2016; **48:** 265–272.
13. Andersson MK, Afshari MK, Andrén Y, *et al*. Targeting the oncogenic transcriptional regulator MYB in adenoid cystic carcinoma by inhibition of IGF1R/AKT signaling. *J Natl Cancer Inst* 2017; **109:** djx017.
14. Andersson MK, Mangiapane G, Nevado PT, *et al*. ATR is a MYB regulated gene and potential therapeutic target in adenoid cystic carcinoma. *Oncogenesis* 2020; **9:** 5.
15. Andersson MK, Åman P, Stenman G. IGF2/IGF1R signaling as a therapeutic target in MYB-positive adenoid cystic carcinomas and other fusion gene-driven tumors. *Cell* 2019; **8:** 913.
16. Ho AS, Kannan K, Roy DM, *et al*. The mutational landscape of adenoid cystic carcinoma. *Nat Genet* 2013; **45:** 791–798.
17. Stephens PJ, Davies HR, Mitani Y, *et al*. Whole exome sequencing of adenoid cystic carcinoma. *J Clin Invest* 2013; **123:** 2965–2968.
18. Andersson MK, Stenman G. The landscape of gene fusions and somatic mutations in salivary gland neoplasms – implications for diagnosis and therapy. *Oral Oncol* 2016; **57:** 63–69.
19. Rettig EM, Talbot CC Jr, Sausen M, *et al*. Whole-genome sequencing of salivary gland adenoid cystic carcinoma. *Cancer Prev Res (Phila)* 2016; **9:** 265–274.
20. Ferrarotto R, Heymach JV. Taking it up a NOTCH: a novel subgroup of ACC is identified. *Oncotarget* 2017; **8:** 81725–81726.
21. Liu B, Mitani Y, Rao X, *et al*. Spatio-temporal genomic heterogeneity, phylogeny, and metastatic evolution in salivary adenoid cystic carcinoma. *J Natl Cancer Inst* 2017; **109:** djx033.
22. Skalova A, Stenman G, Simpson RHW, *et al*. The role of molecular testing in the differential diagnosis of salivary gland carcinomas. *Am J Surg Pathol* 2018; **42:** e11–e27.
23. Ho AS, Ochoa A, Jayakumaran G, *et al*. Genetic hallmarks of recurrent/metastatic adenoid cystic carcinoma. *J Clin Invest* 2019; **129:** 4276–4289.
24. Persson M, Andersson MK, Mitani Y, *et al*. Rearrangements, expression, and clinical significance of MYB and MYBL1 in adenoid cystic carcinoma: a multi-institutional study. *Cancers (Basel)* 2022; **14:** 3691.
25. Persson M, Andren Y, Moskaluk CA, *et al*. Clinically significant copy number alterations and complex rearrangements of MYB and NFIB in head and neck adenoid cystic carcinoma. *Genes Chromosomes Cancer* 2012; **51:** 805–817.
26. Szanto PA, Luna MA, Tortoledo ME, *et al*. Histologic grading of adenoid cystic carcinoma of the salivary glands. *Cancer* 1984; **54:** 1062–1069.
27. Persson F, Winnes M, Andrén Y, *et al*. High-resolution array CGH analysis of salivary gland tumors reveals fusion and amplification of the FGFR1 and PLAG1 genes in ring chromosomes. *Oncogene* 2008; **27:** 3072–3080.
28. Iafrate AJ, Feuk L, Rivera MN, *et al*. Detection of large-scale variation in the human genome. *Nat Genet* 2004; **36:** 949–951.
29. Mermel CH, Schumacher SE, Hill B, *et al*. GISTIC2.0 facilitates sensitive and confident localization of the targets of focal somatic copy-number alteration in human cancers. *Genome Biol* 2011; **12:** R41.
30. Ritchie ME, Phipson B, Wu D, *et al*. limma powers differential expression analyses for RNA-sequencing and microarray studies. *Nucleic Acids Res* 2015; **43:** e47.
31. Mi H, Huang X, Muruganujan A, *et al*. PANTHER version 11: expanded annotation data from gene ontology and reactome pathways, and data analysis tool enhancements. *Nucleic Acids Res* 2017; **45:** D183–D189.
32. Huang da W, Sherman BT, Lempicki RA. Bioinformatics enrichment tools: paths toward the comprehensive functional analysis of large gene lists. *Nucleic Acids Res* 2009; **37:** 1–13.
33. Subramanian A, Tamayo P, Mootha VK, *et al*. Gene set enrichment analysis: a knowledge-based approach for interpreting genome-wide expression profiles. *Proc Natl Acad Sci U S A* 2005; **102:** 15545–15550.
34. Livak KJ, Schmittgen TD. Analysis of relative gene expression data using real-time quantitative PCR and the 2(-Delta Delta C(T)) method. *Methods* 2001; **25:** 402–408.
35. Yusenko MV, Trentmann A, Andersson MK, *et al*. Monensin, a novel potent MYB inhibitor, suppresses proliferation of acute myeloid leukemia and adenoid cystic carcinoma cells. *Cancer Lett* 2020; **479:** 61–70.
36. Rao PH, Roberts D, Zhao YJ, *et al*. Deletion of 1p32-p36 is the most frequent genetic change and poor prognostic marker in adenoid cystic carcinoma of the salivary glands. *Clin Cancer Res* 2008; **14:** 5181–5187.
37. Šteiner P, Andreasen S, Grossmann P, *et al*. Prognostic significance of 1p36 locus deletion in adenoid cystic carcinoma of the salivary glands. *Virchows Arch* 2018; **473:** 471–480.
38. Jost CA, Marin MC, Kaelin WG Jr. p73 is a simian [correction of human] p53-related protein that can induce apoptosis. *Nature* 1997; **389:** 191–194.
39. Karbowski M, Lee YJ, Gaume B, *et al*. Spatial and temporal association of Bax with mitochondrial fission sites, Drp1, and Mfn2 during apoptosis. *J Cell Biol* 2002; **159:** 931–938.
40. Schlisio S, Kenchappa RS, Vredeveld LC, *et al*. The kinesin KIF1Bbeta acts downstream from EglN3 to induce apoptosis and is a potential 1p36 tumor suppressor. *Genes Dev* 2008; **22:** 884–893.
41. Stiewe T, Pützer BM. p73 in apoptosis. *Apoptosis* 2001; **6:** 447–452.
42. Kaghad M, Bonnet H, Yang A, *et al*. Monoallelically expressed gene related to p53 at 1p36, a region frequently deleted in neuroblastoma and other human cancers. *Cell* 1997; **90:** 809–819.
43. Chen ZX, Wallis K, Fell SM, *et al*. RNA helicase a is a downstream mediator of KIF1Bβ tumor-suppressor function in neuroblastoma. *Cancer Discov* 2014; **4:** 434–451.
44. Climent J, Perez-Losada J, Quigley DA, *et al*. Deletion of the PER3 gene on chromosome 1p36 in recurrent ER-positive breast cancer. *J Clin Oncol* 2010; **28:** 3770–3778.
45. Henrich KO, Schwab M, Westermann F. 1p36 tumor suppression-a matter of dosage? *Cancer Res* 2012; **72:** 6079–6088.
46. Cesari R, Martin ES, Calin GA, *et al*. Parkin, a gene implicated in autosomal recessive juvenile parkinsonism, is a candidate tumor suppressor gene on chromosome 6q25-q27. *Proc Natl Acad Sci U S A* 2003; **100:** 5956–5961.
47. Hu HH, Kannengiesser C, Lesage S, *et al*. PARKIN inactivation links Parkinson's disease to melanoma. *J Natl Cancer Inst* 2016; **108:** djv340.
48. Veeriah S, Taylor BS, Meng S, *et al*. Somatic mutations of the Parkinson's disease-associated gene PARK2 in glioblastoma and other human malignancies. *Nat Genet* 2010; **42:** 77–82.
49. Hampe C, Ardila-Osorio H, Fournier M, *et al*. Biochemical analysis of Parkinson's disease-causing variants of Parkin, an E3 ubiquitin-protein

ligase with monoubiquitylation capacity. *Hum Mol Genet* 2006; **15:** 2059–2075.
50. Shimura H, Hattori N, Kubo S, *et al*. Familial Parkinson disease gene product, parkin, is a ubiquitin-protein ligase. *Nat Genet* 2000; **25:** 302–305.
51. Gong Y, Zack TI, Morris LG, *et al*. Pan-cancer genetic analysis identifies PARK2 as a master regulator of G1/S cyclins. *Nat Genet* 2014; **46:** 588–594.
52. Gong Y, Schumacher SE, Wu WH, *et al*. Pan-cancer analysis links PARK2 to BCL-XL-dependent control of apoptosis. *Neoplasia* 2017; **19:** 75–83.
53. Gupta A, Anjomani-Virmouni S, Koundouros N, *et al*. PARK2 depletion connects energy and oxidative stress to PI3K/Akt activation via PTEN S-Nitrosylation. *Mol Cell* 2017; **65:** 1013.e7.
54. Lin DC, Xu L, Chen Y, *et al*. Genomic and functional analysis of the E3 ligase PARK2 in glioma. *Cancer Res* 2015; **75:** 1815–1827.
55. Veeriah S, Morris L, Solit D, *et al*. The familial Parkinson disease gene PARK2 is a multisite tumor suppressor on chromosome 6q25.2-27 that regulates cyclin E. *Cell Cycle* 2010; **9:** 1451–1452.
56. Xiong D, Wang Y, Kupert E, *et al*. A recurrent mutation in PARK2 is associated with familial lung cancer. *Am J Hum Genet* 2015; **96:** 301–308.
57. Ferrarotto R, Mitani Y, McGrail DJ, *et al*. Proteogenomic analysis of salivary adenoid cystic carcinomas defines molecular subtypes and identifies therapeutic targets. *Clin Cancer Res* 2021; **27:** 852–864.
58. Frerich CA, Brayer KJ, Painter BM, *et al*. Transcriptomes define distinct subgroups of salivary gland adenoid cystic carcinoma with different driver mutations and outcomes. *Oncotarget* 2018; **9:** 7341–7358.
59. Phuchareon J, Ohta Y, Woo JM, *et al*. Genetic profiling reveals cross-contamination and misidentification of 6 adenoid cystic carcinoma cell lines: ACC2, ACC3, ACCM, ACCNS, ACCS and CAC2. *PloS One* 2009; **4:** e6040.

SUPPLEMENTARY MATERIAL ONLINE

Figure S1. Overview of the included cohorts of 492/598 analyzable ACCs

Figure S2. Genomic profiling of 100 ACCs

Figure S3. Copy number alterations in ACC

Figure S4. OS of patients with and without 1p36 and 6q deletions detected by arrayCGH

Figure S5. Selected copy number alterations in ACC

Figure S6. siRNA knockdown of early apoptotic genes in 1p36 followed by vinorelbine treatment of ACC cells

Figure S7. *MYB* and *MYBL1* expression in ACCs

Figure S8. Cellular characteristics of cultured ACC67 and ACC100 cells

Table S1. Clinicopathological, genomic, and survival data of 100 ACCs

Table S2. Clinical and pathological characteristics of the ACC patients

Table S3. Recurrent minimal common regions of copy number losses and gains (>10%) in 100 ACCs detected by arrayCGH

Table S4. Peak regions of significant copy number losses involving 1p36.32–p36.22, 6q26, 9p24.1, and 12q13.13 identified by GISTIC2.0

Table S5. Gene amplifications and homozygous deletions in 100 ACCs

Table S6. Significantly downregulated genes in 1p36.32–p36.21 in tumors with 1p36 deletions compared to tumors without deletions

Table S7. Associations of 1p36 and *PARK2* deletions with clinicopathological parameters in 363 ACCs (χ^2 test)

Table S8. Estimation of hazard function of death of ACC patients with Cox regression analysis